BLADES2BUILD PROJECT

D2.5: Computational model for prediction of post-repair lifetime of WTB

WP2

DTU Wind

Funded by
the European Union

TECHNICAL REFERENCES

Grant Agreement Number	101096437
Project Acronym	BLADES2BUILD
Project Title	Recycle, Repurpose and Reuse end-of-life wind blade composites – A coupled pre- and co-processing demonstration
Funding Scheme	HORIZON-CL5-2022-D3-01-02
Project Coordinator	Ana Teresa Macas Lima Technical University of Denmark atmli@dtu.dk
Project Website	www.blades2build.com
Project Duration	January 2023 – December 2025 (36 months)

Deliverable No.	D2.5: Computational model for prediction of post-repair lifetime of WTB
Type / Dissemination level[1]	R or DATA or DEM or OTHER / PU or SEN
Work Package	WP2 - Testing and Identification of Scalable Circularity Frameworks
Task	T2.4 – Repair of wind turbine blades for reuse as blades
Lead beneficiary	DTU Wind
Contributing beneficiary/ies	
Due date of deliverable	30 04 2025
Actual submission date	12 06 2025
Status	Draft or Final

Version	Date	Beneficiary	Author
V1.0	DD/MM/202Y	DTU Wind	Leon Mishnaevsky Jr.

[1]PU – Public, fully open, e.g., web (Deliverables flagged as public will be automatically published in CORDIS project's page)
SEN – Sensitive, limited under the conditions of the Grant Agreement
Classified R-UE/EU-R – EU RESTRICTED under the Commission Decision No2015/444
Classified C-UE/EU-C – EU CONFIDENTIAL under the Commission Decision No2015/444
Classified S-UE/EU-S – EU SECRET under the Commission Decision No2015/444

Authoring and approvals

Prepared		
Name	Organization	Position and title
Name of author i.e. Gaylord Booto	DTU Windi.e. GCS	i.e. GCS Lead

Reviewed			
Name	Organization	Position	Date
	DTU		DD/MM/202Y
	ACCIONA		
	HIC		
	LM WIND		
	NTUA		
	TU/e		
	RWTH AACHEN		
	RENAO		
	CESPA		
	ENDESA		
	PZE		
	GE WIND		
Gaylord Booto	GCS	GCS Lead	
	ELDAN		

Approved			
Name	Organization	Position	Date
Gaylord Booto	GCS	GCS Lead	DD/MM/202Y

DISCLAIMER AND PROPRIETARY RIGHTS STATEMENT

This project has received funding from the European Union's Horizon Europe research and innovation programme under the grant agreement No. 101096437.

Funded by the European Union. Views and opinions expressed are however those of the author(s) only and do not necessarily reflect those of the European Union or the European Climate, Infrastructure and Environment Executive Agency (CINEA). Neither the European Union nor the granting authority can be held responsible for them.

TABLE OF CONTENTS

Technical references 3
Disclaimer and proprietary rights statement 5
Table of contents 6
1 Executive summary 7
2 INTRODUCTION 7
3 MULTISCALE MODEL OF REPAIRED WIND TURBINE BLADE 8
3.1 Full-scale WTB model 8
3.2 Repair model of WTB 11
3.3 RVE sub-model 14
4 POST-REPAIR LIFE PREDICTION MODEL OF WTB 15
4.1 Reliability theory model of structural failure of wind turbine blades 15
4.2 Lifetime prediction of post-repair wind turbine blades 16
5 CONCLUSIONS 17
5.1 Action points 17
5.2 Deviations from DoA 17
6 References 18

1 EXECUTIVE SUMMARY

The task team tried several times to reach the LM/GE partner team, but they did not respond and could not provide the information about their methods of prediction of repaired blade lifetime.

Repair and maintenance operations of wind turbines constitute a significant part of costs of wind energy. In this paper, technologies of structural repair of damaged wind turbine blades are reviewed. Technologies of repair are compared, including hand layup lamination, vacuum repair with hand layup and infusion, ultraviolet repair and high temperature thermal curing. Computational models of repaired blades, and curing as kinetic process are presented. Void formation during repair and curing, and the void influence on the post-repair reliability of blades is discussed. Further, technologies of repair of new generation of recyclable wind turbine blades are also discussed.

Keywords: Repair of wind turbine blades; New generation of new wind turbine blades; Repair technology

2 INTRODUCTION

A second lifecycle of wind turbines abroad has been identified by performing expert interviews, and reselling turbines for a second lifecycle in Denmark is approximately 60 % [1]. This trend is expected to persist due to the high cost of decommissioning wind turbines. Although most wind turbine blades are structurally capable of operating well beyond their initially estimated service life, leading edge damage often occurs much earlier. Consequently, blade repair becomes a critical technology for ensuring the successful and efficient life extension of wind turbine blades. In order to ensuring operational reliability and cost efficiency, the life prediction of post-repair wind turbine blades is critical.

Blade repair often introduces material heterogeneities, altered stress distributions, and residual defects that compromise the original WTB design integrity [2,3]. Furthermore, repaired regions are susceptible to accelerated degradation under cyclic loads due to surface roughness variations, incomplete curing of resins, or mismatched material properties between the original and repaired sections [4,5], which requires tailored predictive frameworks that account for post-repair structural dynamics. Finite element analysis (FEA) , validated with field measurements, is a promising method to model real-time load redistributions and monitor accumulation in repaired blades [3,6] and improve lifetime estimates [2].

3 MULTISCALE MODEL OF REPAIRED WIND TURBINE BLADE

3.1 Full-scale WTB model

To achieve a realistic boundary condition, a full-scale finite element wind blade model was firstly established. The numerical model of the geometry of the DTU 12.6 m wind turbine blade is derived from a basic structural blade model defined in DTU's in-house software: Blade Modelling Tool (BMT) [7]. The commercial finite element software Abaqus/CAE is used as a pre/post-processor with Abaqus/Standard as a solver. The entire blade geometry was modelled based on input data of 99 blade cross-sections generated by DTU's Wind HawtOpt2 [8] optimization toolchain defining the airfoil. These cross-sections describe the outer geometry (airfoil) of the blade. For the discretization with conventional shell elements, the aerodynamic blade profile is used as the reference surface, with the shell normal pointing from the reference surface towards the inner part of the blade. Simultaneously, an offset of half of the shell thickness from the shell's mid-surface is applied to ensure that the aerodynamic surface is the reference surface. No offset is chosen for the shear webs, meaning that the geometrical middle of the shear webs is used as the reference surface. For the modelling approaches based on a volumetric geometry representation, cross-section curves are offset from the airfoil according to the layup definition representing the thickness of laminates [9].

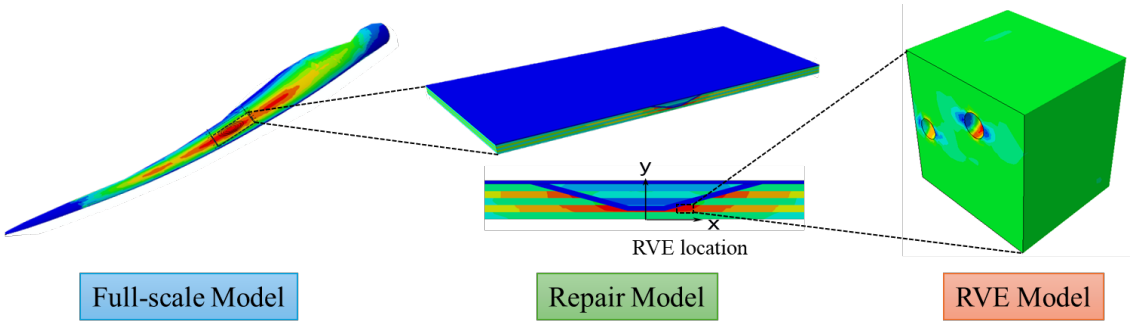

Figure 1 Description of sequential multiscale modeling of wind turbine blade.

Each cross-section consists of 60 regions/sections to discretize the different cross-sectional properties and possible changes in the layup of the composite structure. The composite layup consists of 6 to 54 plies through the thickness, in which the material properties, layup and ply orientations are assigned automatically by the BMT. Subsequently, the 2D cross sections, defined by their airfoil and the shear web shape at specific positions along the wind turbine blade span, are connected via a 3D lofting feature, creating a three-dimensional blade structure.

Figure 2 shows the modelling approach of the trailing edge region. The modelling approach used here modelled the trailing edge as a combined shell-solid element modelling approach [10], where the solid elements were added to the structure which represented the adhesive bondline to link and

stiffen the region. Figure 2(a) demonstrates the shell model, and Figure 2(b) is the shell model which includes the presented shell thickness rendering.

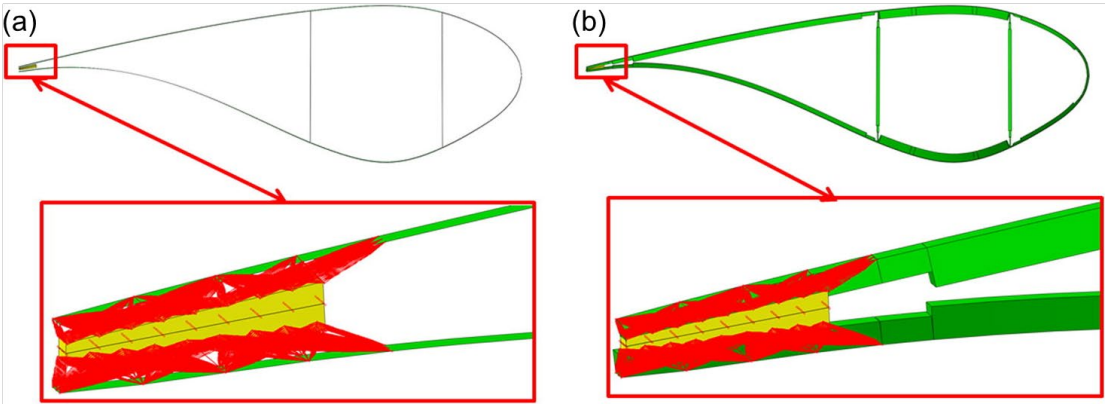

Figure 2 Coss sectional view of the blade trailing edge region [10].

As illustrated in Figure 3 and Figure 4, a kinematic (rigid) coupling constraint was applied to the nodes of the root section. All six degrees of freedom of the master node located in the elastic centre of the root section were restrained. The four anchor plates were assumed to be rigid and hence, modelled through kinematic coupling constraints tied to the master nodes of each loading point. For model validation, the load was applied by axial contraction of connector elements. This follower force approach is a realistic representation of the experimental loading conditions. Axial connector elements were also used to model the draw wire transducer (ASM) measurement principle, thereby enabling a direct comparison between measurements and numerical results.

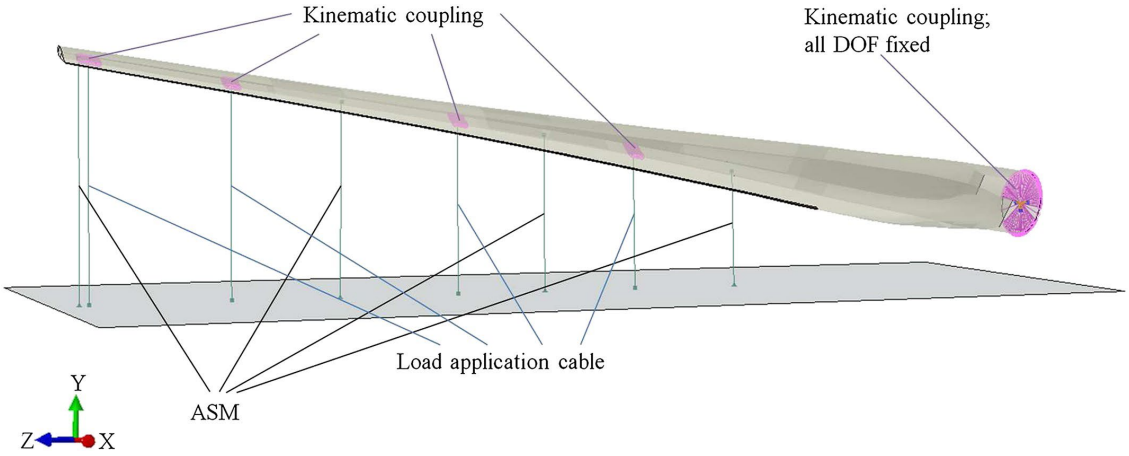

Figure 3 Wind turbine blade model simulating test conditions for validation. Boundary conditions at the root and both loading points and ASMs modelled with axial connector elements tied to the strong floor. DOF, degrees of freedom [11].

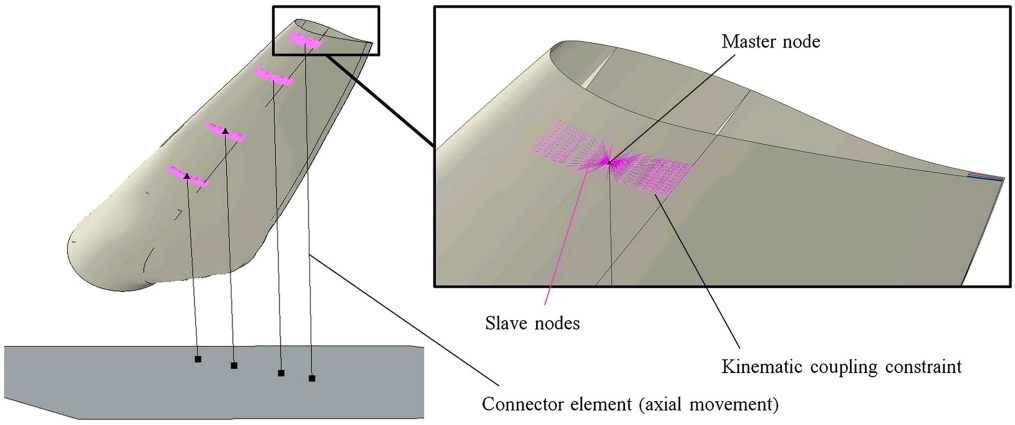

Figure 4 Details of kinematic coupling constraints used to model the loading conditions similar to the blade test [11].

All numerical simulations were performed as quasistatic simulations including geometric non-linearity. For most of the simulations, the Abaqus standard Newton–Raphson solver technique was used. In load cases associated with geometrically non-linear wave formation, equilibrium could not be reached with the standard solver for higher loads. In order to overcome these convergence problems, an implicit dynamic solver was chosen instead. The loads were linearly ramped up over a period of 10 s so the kinetic energy was at least two orders of magnitude smaller than the strain energy in each time increment. A viscosity coefficient of 10-4 was used to stabilize the numerical simulations.

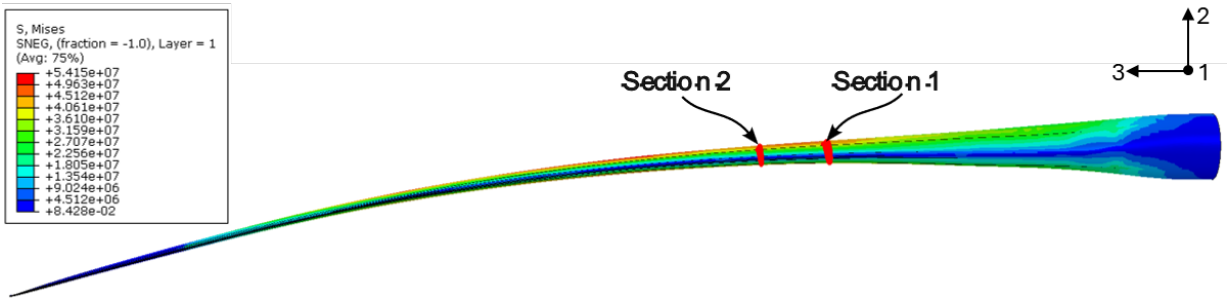

Figure 5 Mises stress distribution in the full-scale wind blade model

Figure 5 shows the stress field in the full-scale model. It can be obtained that the maximum von Mises stresses occur at a span location of 4 m from the root of the wind turbine blade. Since leading-edge damage is one of the main damage mechanisms affecting WTB, it was introduced at the maximum von Mises stress location as demonstrated in Figure 6(a).

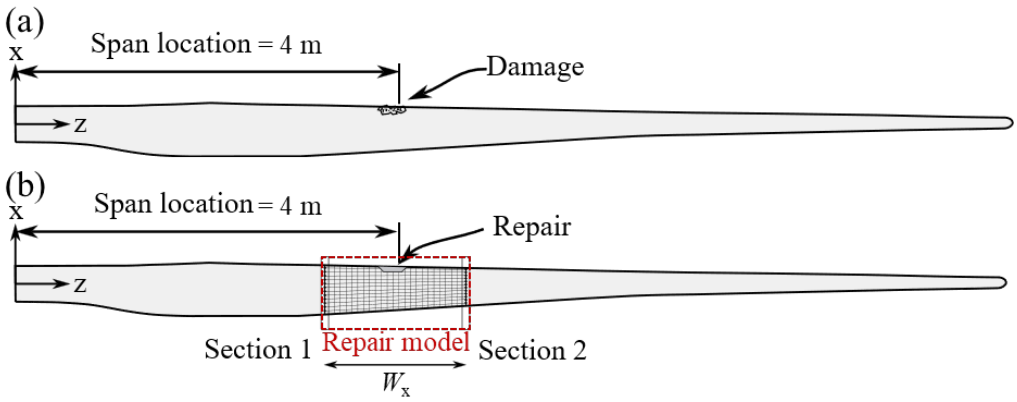

Figure 6 (a) Location of leading-edge damage; (b) Location of repair model.

The area around the damage is used to establish the repair model. As demonstrated in Figure 6(b), node displacements at section 1 and section 2 in different directions are extracted and the differences of displacements are plotted in Figure 7. Since the relative displacements are different along the chord of the blade (e.g., there's larger relative displacements at the trailing edge than at the leading edge), the maximum value of the relative displacements in the direction of the span of the blade is used as the boundary conditions for the repair model.

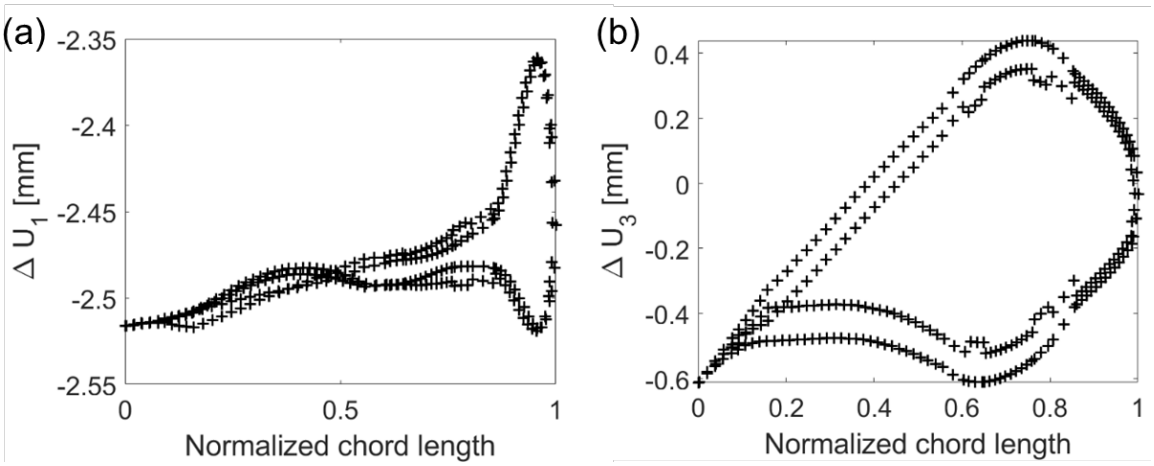

Figure 7 Relative difference of displacement between section 1 and section 2: (a) in the 1-direction; (b) in the 3-direction.

3.2 Repair model of WTB

A Python tool was developed for generating a 3D FEM model of a coating/scarf/adhesive/parent structure [12]. The input for the Python tool consists of several geometric, material, and modelling parameters. The dimensions for the repair geometry are chosen so that they are consistent with the dimensions of a 12 m blade. Moreover, the materials and layup of the assumed damaged region are also consistent with the layup of the full-scale blade at the leading edge and span of 4 m. The details of modeling information is given in Table 1.

Table 1 Information of the geometry model

Description	Symbol	Value	Unit
Number of layers	n	9	-
Layer thickness	t_l	0.4	mm
Repair angle	α_0	22	deg.
Safe distance angle	α_{min}	3	deg.
Adhesive thickness	t_a	0.6	mm
Lower radius	r_{low}	40	mm
Upper radius	r_{up}	43.71	mm
Width x-direction	W_x	250	mm
Width z-direction	W_z	250	mm

A schematic of the repaired geometry is given in Figure 8. The laminate for the repair model is defined by the blade model corresponding to the region of the leading edge at a span of 4 m.

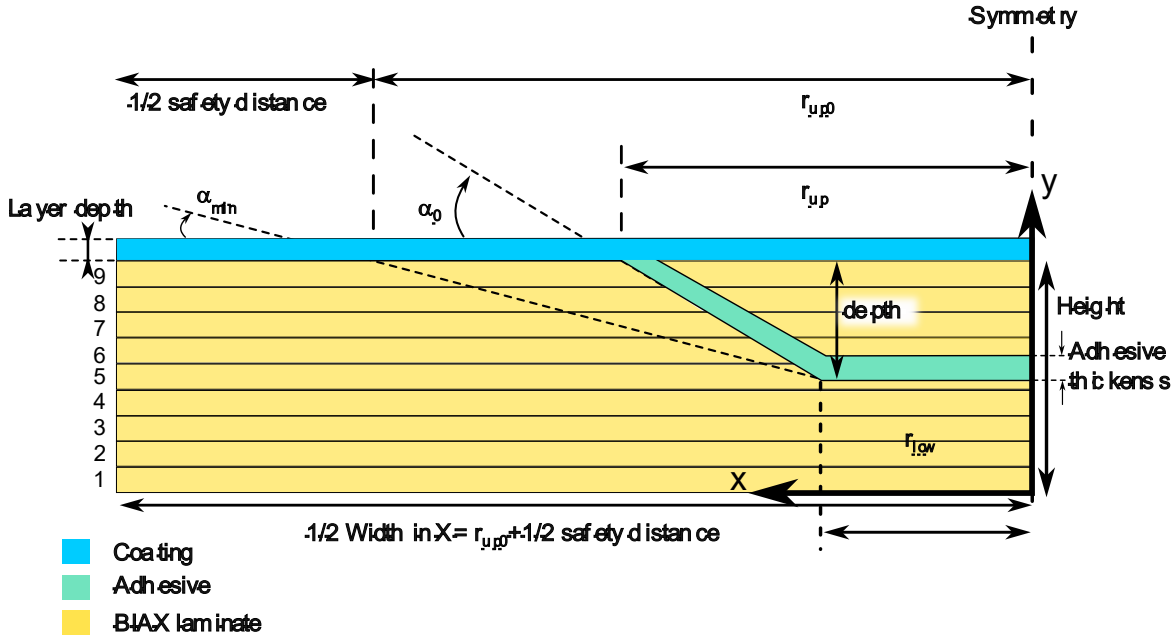

Figure 8 Lay-up sequences of the repair model.

The material properties of the coating, adhesive, and BIAX laminate are shown in Table 2.

Table 2 Material properties used in the repair model

Material	Young modulus (Gpa)	Poisson's ratio
Coating, polyurethane	0.3	0.3
Adhesive, epoxy	3.0	0.3
Biaxial (BIAX) laminate	13.92/13.92/13.92	0.53/0.53/0.26

The geometry model is discretized with element C3D8R in the coating and element C3D4 in the adhesive and laminate. The mesh is generated by imposing uniform seeds on the model edges and on the circumference of each cut layer. A mesh sensitivity study was carried out to obtain the optimum mesh size as presented in Figure 9(a).

The boundary conditions of the repair model are shown in Figure 9(b). The model is fixed in the x direction at one end, and the rotations about the y-axis and z-axis are also fixed on the same face. At the other end, a displacement is imposed on a master node which is coupled with the rest nodes at the opposite side of the fixed boundary conditions.

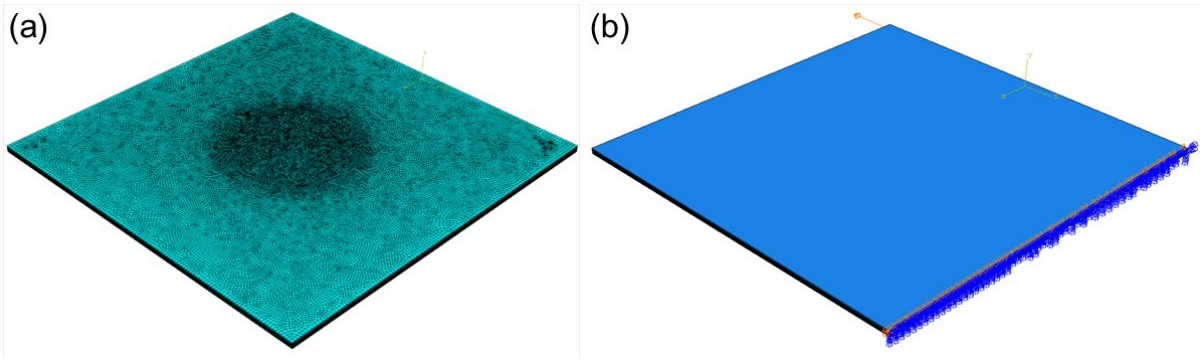

Figure 9 Repair model: (a) Mesh; (b) Boundary conditions.

A mesh sensitivity study was carried out using the maximum von Mises value of the entire repair model. A mesh independent result can be obtained with approximately 1.65 million elements as shown in Figure 10.

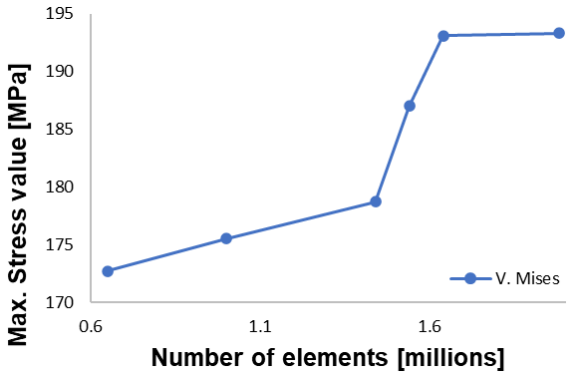

Figure 10 Mesh sensitivity analysis of repair model.

Contour plots with von Mises stresses of the repair model are shown in Figure 11.

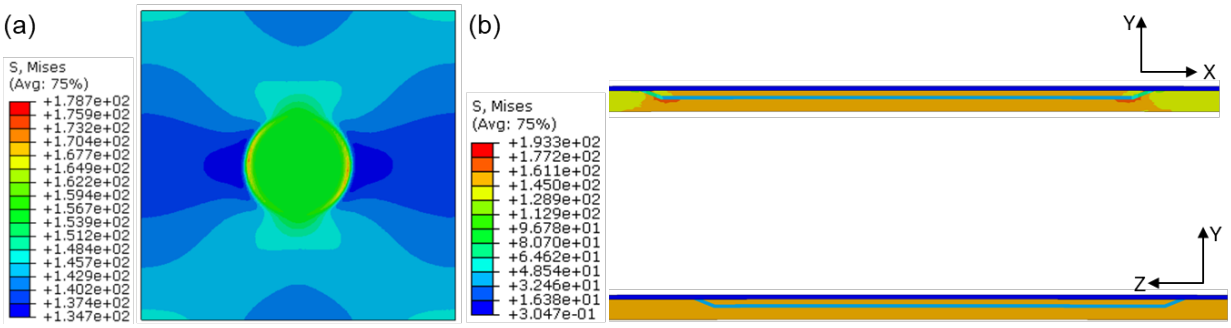

Figure 11 Von Mises stress of the repair model: (a) In-plane; (b) Through thickness.

3.3 RVE sub-model

To establish a connection from the repair model to the RVE model, a sub-model approach is used. In general, the solid-to-solid sub-modelling technique is used to obtain more accurate results in a localized region of a model by using a refined mesh (the sub-model) within a larger, coarser model (the global model). It should be noted that the same approach for extracting boundary conditions cannot be applied, primarily due to factors such as the idealized nature of the repair geometry.

The representative volume element (RVE) model, serving as a sub-model of the global repair model, is generated using a Python script. The RVE is constructed as a cube with side lengths of 0.5 mm. To model the effect of resin voids, the RVE is modified by removing material using Boolean operations. The voids are idealized as perfect spheres of 0.05 mm radius, and their position is randomly assigned inside the RVE (the location is restricted in a way that the voids are fully inside the RVE). The material properties are linked to the location of the RVE within the global model. In this study, the RVE is positioned at the region where the BIAX laminate and the adhesive exhibit the highest von Mises stress. No RVE is assigned to the coating, as its stress level is negligible.

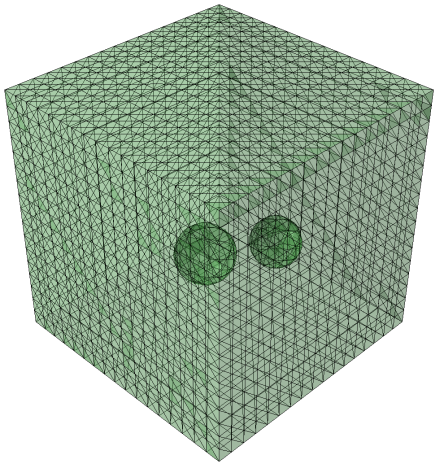

Figure 12 RVE sub-model with two voids

In Figure 12, two voids are shown, however, the tool can generate any number of voids in the RVE volume. This is particularly useful to study the effect of void content and the effect of void interaction. The relationship of maximum stress and void content is shown in Figure 13.

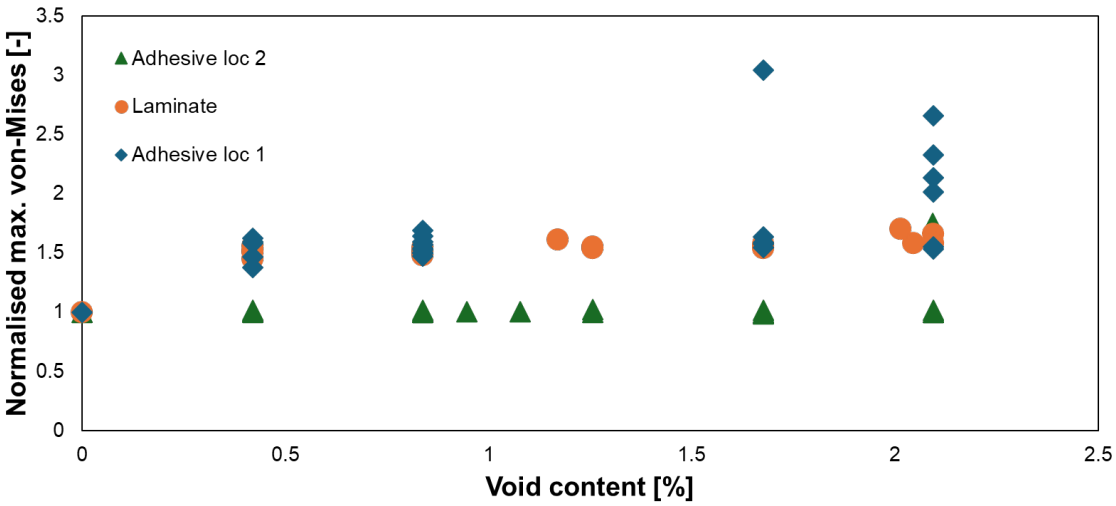

Figure 13 Variation of maximum Mises stress with increasing void content.

4 POST-REPAIR LIFE PREDICTION MODEL OF WTB

4.1 Reliability theory model of structural failure of wind turbine blades

The root causes of wind turbine blade failure were reviewed and analyzed in [13]. Therefore, if putting apart the lightning and leading edge erosion damage mechanisms (which are most often observed, on the one side, but weakly related to the resin used in laminates), the blade failure process can be described as follows. Laminates are subject to stress loading cycles, and local defects (like voids or microcracks) increase local stresses. For significant part of the blade lifetime, the stresses (also local stresses near defects) are below the endurance limit. However, if the loads are high enough, local degradation can be triggered, first at microlevel, and then at macrolevel. Combination of high external loads and big manufacturing defects in critical regions leads to the blade failure. The level of local stresses is controlled by voids in this region, external load, and residual stresses. A special case is the post-repair blade failure. After the first failure, a wind turbine blade is subject to a repair, i.e. removal of damaged region, grinding, attachment of scarf, curing and gluing. Repair procedures also lead to formation of defects (voids, new interfaces, residual stresses) in the composite structure [14,15].

Failure of wind turbine blade is considered as occurrence of one of several common failure events: (A) collapse or buckling, (B) failure of adhesive joints, (c) failure of repaired region and (d) delamination at plydrop [13]. Considering wind turbine blade as multielement structure, one can determine the probability of failure of wind turbine blades as a combination (sum or multiplication) of failure probabilities of its elements. Assuming the degradation processes in the laminates and

adhesives are independent, the probability of structural failure of blade can be estimated as shown in Figure 14.

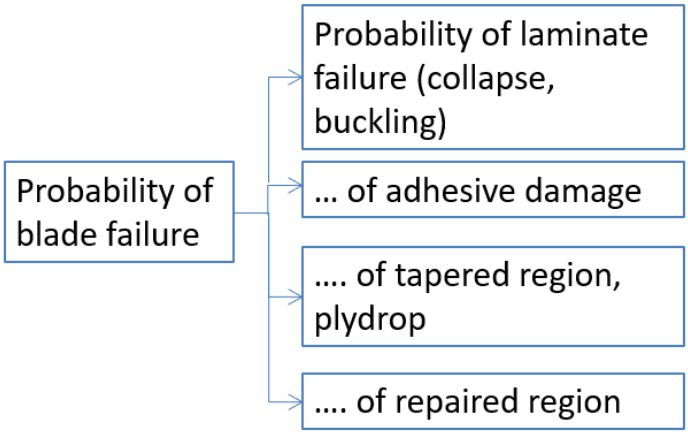

Figure 14 Schema: Probability of blade failure based on expected failure mechanisms.

4.2 Lifetime prediction of post-repair wind turbine blades

In the following, we neglect the likelihood of "secondary" failure of repaired blade and assume that most critical element of repaired blade is the repaired area. The blade is assumed to be subject to random cyclic load, with load level following Gaussian distribution. The local load on the repaired region is assumed to be proportional to the load on the blade.

Local failure occurs when the local stresses (or another damage criterion, e.g. plastic or elastic strain) near available manufacturing defects exceed some critical level for given resin material, damage grows and forms a crack, comparable to the structural element dimensions (e.g., adhesive layer thickness). Taking into account the random component of the damage and stress, the failure condition for epoxy resin can be described using the two parameter Weibull distribution [16]:

$$Prob\{Local_{failure}\} = 1 - \exp\left(-\left(\frac{f}{f_{cr}}\right)^{m}\right)$$

where $f_{cr}$is the scale parameter and m is termed the shape parameter or the Weibull modulus, f – failure measure, for instance, stress (f=σ). Assuming the load on the blade, as a stationary random value, following Gaussian distribution, one can determine time to failure of a blade as follows. We approximate failure as the first up-crossing of a critical load. Then we compute the up-crossing rate, using Rice's formula. The mean time to failure is given by a complex formula and is proportional to

$$t_F \sim \exp\left(\frac{(\sigma_{cr} - \sigma_{av})^2}{2s^2}\right)$$

Where σ_{av} and s – mean and standard deviation of stress in repaired area, σ_{cr}- critical stress in repaired area. σ_{av} and s are parameters of blade loading, and do not depend on repair quality and

conditions. However, σ_{cr}, critical stress at which failure occurs, strongly depends on the repair quality, first of all, on defects in the repaired part. The local stress concentration near the voids is an increasing function of the void size. To simplify the void effect analysus, we use the effective stress concept from damage mechanics, with stress multiplied by 1/(1-D), where D – damage parameter, here, void density: $\sigma_{cr,voided\ material} = \sigma_{cr,ideal\ material}/(1-D)$.

Let us consider an ideal case of a material without voids or other defects and assume that the lifetime of blade produced from such material equals t_{ideal} (for instance, t_{ideal} can be taken as 50 years for epoxy based common blades). The real lifetime is reduced, due to the defects in the blade, and in particular, due to defects caused by repair procedures (here, neglecting the blade defects formed during manufacturing). Then, one can determine the lifetime of blade after repair as a function of density of voids in the repaired region:

$$t_F = t_{ideal}\exp\left(\frac{(\sigma_{cr}/(1-D)-\sigma_{av})^2-(\sigma_{cr}-\sigma_{av})^2}{2s^2}\right)$$

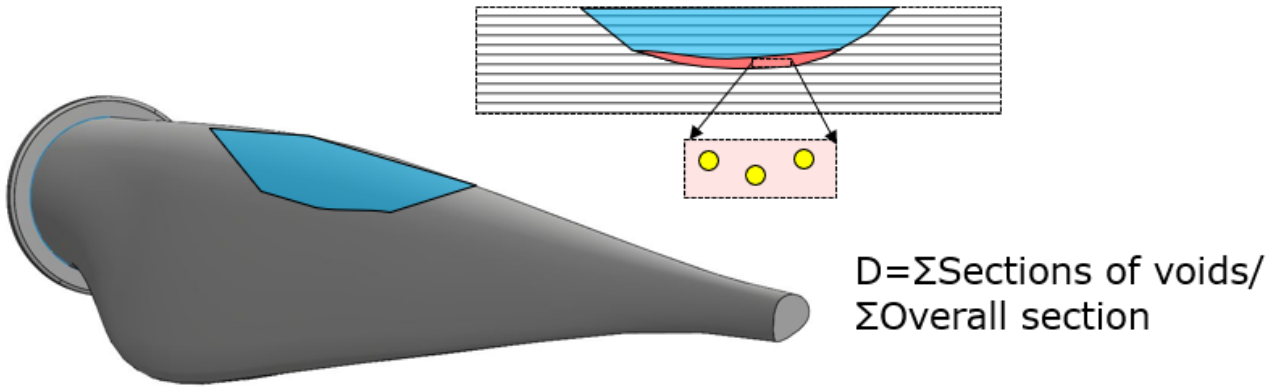

Figure 15 Schema: Voids in repaired region of blade and damage parameter

5 CONCLUSIONS

Multiscale computational model for the calculation of post-repair lifetime of wind turbine blades is developed. The validation of the model is underway.

5.1 Action points

Validation of the developed method of post-repair lifetime prediction for repaired blades

5.2 Deviations from DoA

No deviations

6 REFERENCES

[1] K.J. Kramer, A.B. Abrahamsen, J. Beauson, U.E. Hansen, N.-E. Clausen, A.P.M. Velenturf, M. Schmidt, Quantifying circular economy pathways of decommissioned onshore wind turbines: The case of Denmark and Germany, Sustainable Production and Consumption 49 (2024) 179–192. https://doi.org/10.1016/j.spc.2024.06.022.

[2] M. Grujicic, G. Arakere, E. Subramanian, V. Sellappan, A. Vallejo, M. Ozen, Structural-Response Analysis, Fatigue-Life Prediction, and Material Selection for 1 MW Horizontal-Axis Wind-Turbine Blades, J. of Materi Eng and Perform 19 (2010) 790–801. https://doi.org/10.1007/s11665-009-9558-8.

[3] J. Gebel, A. Rezaei, P.-J. Daems, R. Marini, J.-J. Matthys, A.R. Nejad, J. Helsen, Wind turbine blade root and blade bearing fatigue damage estimation based on field data, Forsch Ingenieurwes 89 (2025) 16. https://doi.org/10.1007/s10010-025-00789-z.

[4] H.J. Kim, J.-R. Cho, Numerical Analysis of Fatigue Life of Wind Turbine Blades Reinforced with Graphene Platelets, Applied Sciences 15 (2025) 1866. https://doi.org/10.3390/app15041866.

[5] B. Loza, J. Pacheco-Chérrez, D. Cárdenas, L.I. Minchala, O. Probst, Comparative Fatigue Life Assessment of Wind Turbine Blades Operating with Different Regulation Schemes, Applied Sciences 9 (2019) 4632. https://doi.org/10.3390/app9214632.

[6] X. Gao, H. Ying, L. Li, Z. Chang, M. Kong, X. Tian, Prediction of Fatigue Life at the Root Section of Offshore Single-Pile Wind Turbine Tower, Journal of Marine Science and Engineering 13 (2025) 620. https://doi.org/10.3390/jmse13030620.

[7] P.U. Haselbach, P. Berring, A. Larionova, S. Semenov, A.M. Antunes, M. Hedayatzadeh, K. Branner, Quantifying the accuracy of different modelling techniques and element types to predict the structural performance of the DTU 12.6m wind turbine blade: 21st European Conference on Composite Materials, Proceedings of ECCM21 – 21st European Conference on Composite Materials 3 (2024) 1293–1300.

[8] F. Zahle, C. Tibaldi, D.R. Verelst, R. Bitche, C. Bak, Aero-Elastic Optimization of a 10 MW Wind Turbine, (2015). https://doi.org/10.2514/6.2015-0491.

[9] J.P. Blasques, User's Manual for BECAS: A cross section analysis tool for anisotropic and inhomogeneous beam sections of arbitrary geometry, Risoe DTU - National Laboratory for Sustainable Energy, 2012.

[10] P.U. Haselbach, An advanced structural trailing edge modelling method for wind turbine blades, Composite Structures 180 (2017) 521–530. https://doi.org/10.1016/j.compstruct.2017.08.029.

[11] P.U. Haselbach, M.A. Eder, F. Belloni, A comprehensive investigation of trailing edge damage in a wind turbine rotor blade, Wind Energy 19 (2016) 1871–1888. https://doi.org/10.1002/we.1956.

[12] L. Mischnaewski III, L. Mishnaevsky Jr, Structural repair of wind turbine blades: Computational model for the evaluation of the effect of adhesive properties, Wind Energy 24 (2021) 402–408. https://doi.org/10.1002/we.2575.

[13] L. Mishnaevsky, Root Causes and Mechanisms of Failure of Wind Turbine Blades: Overview, Materials (Basel) 15 (2022) 2959. https://doi.org/10.3390/ma15092959.

[14] D. Paul, A. Varshney, P. Mahajan, L. Mishnaevsky, Post-repair residual stresses and microstructural defects in wind turbine blades: Computational modelling, International Journal of Adhesion and Adhesives 123 (2023) 103356. https://doi.org/10.1016/j.ijadhadh.2023.103356.

[15] A. Varshney, D. Paul, P. Mahajan, L. Mishnaevsky, Cure-induced residual stresses and viscoelastic effects in repaired wind turbine blades: Analytical-numerical investigation, Composites Part C: Open Access 15 (2024) 100521. https://doi.org/10.1016/j.jcomc.2024.100521.

[16] A. Tempelis, L. Mishnaevsky, Coating material loss and surface roughening due to leading edge erosion of wind turbine blades: Probabilistic analysis, Wear 566–567 (2025) 205755. https://doi.org/10.1016/j.wear.2025.205755.